optica

Wavelength-scale optical parametric oscillators

Saman Jahani, Arkadev Roy, and Alireza Marandi*

Department of Electrical Engineering, California Institute of Technology, Pasadena, California 91125, USA
**Corresponding author: marandi@caltech.edu*

Received 6 October 2020; revised 10 December 2020; accepted 17 January 2021 (Doc. ID 411708); published 19 February 2021

Despite recent progress in nonlinear optics in wavelength-scale resonators, there are still open questions on the possibility of parametric oscillation in such resonators. We present a general approach to predict the behavior and estimate the oscillation threshold of multi-mode subwavelength and wavelength-scale optical parametric oscillators (OPOs). As an example, we propose an OPO based on Mie-type multipolar resonances, and we demonstrate that due to the low-Q nature of multipolar modes in wavelength-scale resonators, there is a nonlinear interaction between these modes. As a result, the OPO threshold, compared to the single-mode case, can be reduced by a factor that is significantly larger than the number of interacting modes. The multi-mode interaction can also lead to a phase transition manifested through a sudden change in the parametric gain as well as the oscillation threshold, which can be utilized for enhanced sensing. We establish an explicit connection between the second-harmonic generation efficiency and the OPO threshold. This allows us to estimate the OPO threshold based on measured or simulated second-harmonic generation in different classes of resonators, such as bound states in the continuum and inversely designed resonators. Our approach for analyzing and modeling miniaturized OPOs can open unprecedented opportunities for classical and quantum nonlinear photonics.

https://doi.org/10.1364/OPTICA.411708

1. INTRODUCTION

Optical parametric oscillators (OPOs) have been used widely for may applications ranging from metrology and spectroscopy to quantum information science [1–9]. OPOs consist of a medium with quadratic or Kerr nonlinearity within a resonator, which is typically much larger than the operation wavelength, converting pump photons to signal and idler photons [2–7]. At degeneracy, the indistinguishable signal and idler of an OPO can form a squeezed vacuum state below the oscillation threshold [10,11] and have been used for several applications in quantum information processing [9,12–14]. Above threshold, the conversion efficiency boosts rapidly and the output signal illustrates a binary phase state that can be utilized as a spin in an artificial Ising network [15,16]. Above-threshold degenerate OPOs have also been effectively used for generation of mid-IR frequency combs [4,8,17].

Recent progress in nanoscale light confinement as well as precise nanofabrication of challenging nonlinear materials [18,19] have inspired the idea of rethinking the possibilities of miniaturization of nonlinear systems to their extreme. Miniaturized OPOs have recently been demonstrated in on-chip OPOs based on Kerr [5,6,20] and quadratic [21] nonlinearities as well as whispering-gallery resonators [22]. The sizes of these resonators are still orders of magnitude larger than their operating wavelengths. Strong field confinement inside nanostructures has shed light on the possibility of nonlinear optics at nano-scale [23–28]. However, the main focus so far has been devoted to up-conversion in nanostructures, while optical parametric oscillation in wavelength-scale structures is still unexplored. Conventional theories that have been developed mostly for traveling-wave nonlinear optical systems [29] or high-Q resonators [30,31] cannot be applied directly to accurately model OPOs in nano-structures. The reason is that the spatial variation of the field happens in the subwavelength regime where slowly varying envelope approximation (SVEA) is not valid anymore [29]. Moreover, unlike conventional large-scale OPOs, in nano-structured resonators, the input pump can excite several modes of the cavity at the pump wavelength, and due to the low-Q nature of modes, the pump can also directly interact with several modes at the signal wavelength. A few theoretical models have been proposed recently to explain the spontaneous down-conversion in Mie resonators [32,33] and the threshold in 2D materials-based OPOs [34]. However, these theories are either limited to specific structures or cannot explain the behavior of the system above the threshold.

Here, we derive general conditions of parametric oscillation in subwavelength and wavelength-scale resonators. In the low-Q regime of these resonators, multiple modes around the signal wavelength can spectrally and spatially overlap (Fig. 1). This allows them to nonlinearly interact with each other through the pump. As an example, we estimate the OPO threshold in an AlGaAs nanoparticle that supports Mie-type multipolar resonances. We show that the multi-mode interactions at the signal wavelength can lead to a significant reduction in the threshold by a factor remarkably higher than the number of modes. The multi-mode interactions also result in a phase transition from degenerate to non-degenerate in these resonators with an abrupt change in the parametric gain and/or oscillation threshold, which can be utilized for ultra-sensitive measurements. Moreover, we establish a

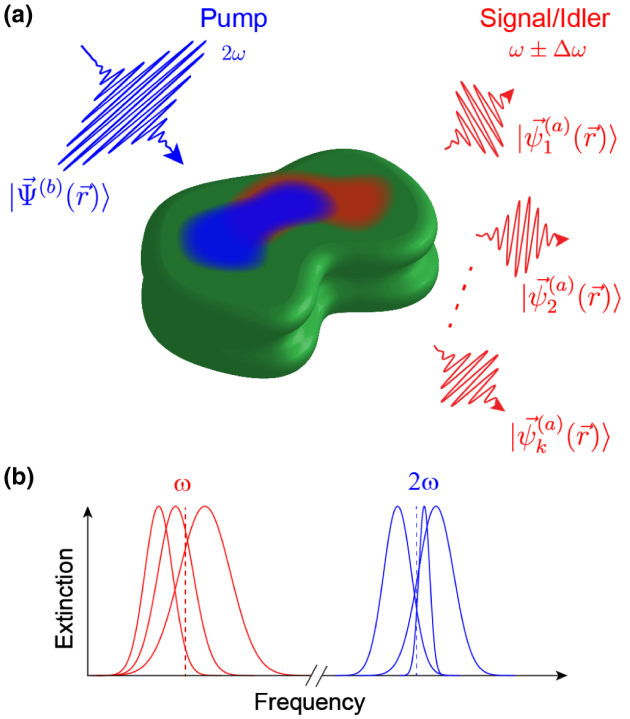

Fig. 1. Wavelength-scale optical parametric oscillators (OPOs). (a) OPO with arbitrary geometry that resonates around the pump frequency (2ω) and the half-harmonic ($\omega \pm \Delta\omega$). (b) Nonlinear behavior of the OPO can be determined by knowing the spatial overlap between the pump excitation at 2ω and eigenmodes of the cavity around ω as well as the linear properties of the cavity around the pump and signal frequencies.

connection between up-conversion processes in nanostructures and parametric down-conversion. This allows us to explore the possibility of OPO in existing structures that have been offered for sum-frequency/second-harmonic generation (SHG). Our approach is general and can predict optical parametric oscillation in a wide range of nanostructured resonators, such as bound states in the continuum, photonic crystal, and inversely designed cavities.

2. THEORY

To estimate the OPO threshold in multi-mode wavelength-scale resonators, we expand the field inside the cavity in terms of orthogonal eigenmodes [Fig. 1(a)], and we approximate the nonlinear dynamics of the electric field with a slowly varying envelope evolving in time domain (see Supplement 1 for more details). The electric field for the signal, idler, and pump can be expanded as the superposition of the quasi-normal modes as $\vec{E}(\vec{r},t) = \mathcal{E}_a \sum_k a_k(t) e^{-i(\omega - i\frac{\alpha_k}{2})t} |\vec{\psi}_k(\vec{r})\rangle + \text{c.c.}$, where a_k is the slowly varying envelope [35–37], $\mathcal{E}_a$ is the normalization constant such that $|a_k|^2$ is the energy stored in the kth mode of the cavity, and for a homogeneous resonator, it is $\mathcal{E}_a = \sqrt{2/\varepsilon_0 n(\omega)^2}$, $|\vec{\psi}_k(\vec{r})\rangle$ are the cavity quasi-normal modes normalized such that $\langle \vec{\psi}_m(\vec{r}) \vec{\psi}_k(\vec{r})\rangle = \delta_{mk}$ (δ_{mk} is the Kronecker delta), ω is the angular frequency of the signal (ω_s), idler (ω_i), or pump (ω_p), $\alpha_k = \omega_k / Q_k$ is the decay rate of the cavity mode, ω_k is the eigenfrequency of the kth mode with a quality factor of Q_k, and $\delta\omega_k = \omega - \omega_k$ is the detuning of the center of resonance of kth from the frequency of the electromagnetic field.

The wave equation for each of the signal modes is simplified to (see Supplement 1)

$$\frac{d}{dt} a_l^{(s)} = \left(i\delta\omega_l^{(a)} - \frac{\alpha_l^{(a)}}{2} \right) a_l^{(s)} + ib \sum_k \eta_{lk} a_k^{(i)*}, \tag{1}$$

where $a^{(s)}$, $a^{(i)}$, and b represent signal, idler, and pump envelope, respectively. $i\delta\omega_l^{(a)}$ and $\alpha_l^{(a)}$ are the detuning and the decay rate for the signal/idler modes, respectively, and η_{lk} is the nonlinear coupling between the lth mode and kth mode as

$$\eta_{lk} = \omega \langle \frac{\mathcal{E}_b \chi^{(2)}}{n(\omega)^2} \vec{\psi}_l^{(a)*}(\vec{r}) \vec{\Psi}^{(b)}(\vec{r}) \vec{\psi}_k^{(a)*}(\vec{r}) \rangle. \tag{2}$$

Note that the pump mode, $b(t)|\vec{\Psi}^{(b)}(\vec{r})\rangle$, is a superposition of modes at the pump wavelength, which is dictated by the input excitation. However, the signal has to be expanded to the quasi-normal modes (see Supplement 1). Equation (1) combined with a similar equation governing the idler dynamics can be written in a matrix form as

$$i\frac{d}{dt}\boldsymbol{\mathcal{A}}(t) = \boldsymbol{\mathcal{H}}(b)\boldsymbol{\mathcal{A}}(t), \tag{3}$$

where $\boldsymbol{\mathcal{A}}(t) = \left[a_1^{(s)}, a_1^{(i)*}, \ldots, a_k^{(s)}, a_k^{(i)*}, \ldots\right]^T$. The electric field can be expressed as a superposition of the eigenmodes as

$$\vec{E}_\omega(\vec{r},t) = e^{-i\omega t} \sum_m \Big(e^{-i\lambda_m t} \sum_k a_{k,m}^{(s)} |\vec{\psi}_k^{(a)}(\vec{r})\rangle + e^{+i\lambda_m^* t} \sum_k a_{k,m}^{(i)*} |\vec{\psi}_k^{(a)}(\vec{r})\rangle \Big) + \text{c.c.}, \tag{4}$$

where $[\lambda_m]$ are the eigenvalues, and $\vec{V}_m = [a_{k,m}^{(s,i)}]$ are the corresponding eigenvectors of the Hamiltonian ($\boldsymbol{\mathcal{H}}$), which define the signal/idler supermodes. A supermode starts to oscillate when the imaginary part of the corresponding eigenvalue ($\text{Im}(\lambda_m)$) surpasses zero. The minimum pump power to reach this condition defines the oscillation threshold. The real part of the eigenvalues corresponds to the signal and idler frequency separation from the half-harmonic ($\text{Re}(\lambda_m) = \Delta\omega$; $\omega_{s,i} = \omega \pm \Delta\omega$). Hence, the eigenvalues for degenerate OPOs ($\omega_s = \omega_i = \omega_p/2$) are purely imaginary, and they are complex for non-degenerate cases.

3. RESULTS

Our model is general and can be applied to a wide range of resonators. First, we apply our model to estimate the threshold in an AlGaAs sphere [Fig. 2(a)]. The reason that we have chosen this simple structure is that the eigenmodes for this structure can be derived analytically and be expressed as multipolar resonances [38,39]. Since the modes for a wide range of nanostructures, such as cylinders and cubes, can be expressed as multipolar resonances as well, our results can shed some light on the possibility of OPO in similar structures that are more amenable to fabrication on a chip [40–48]. Also, AlGaAs is a low-loss high-index ($\varepsilon \approx 10$) material at optical frequencies with strong second-order nonlinearity ($\chi_{ijk}^{(2)} = 200$ pm/V, $i \neq j \neq k$) [49], and with appropriate orientation [50], it has been recently explored for strong SHG at nanoscale [23,45–47,49]. Hence, it is an excellent candidate for demonstration of OPO at wavelength-scale with a relatively low threshold.

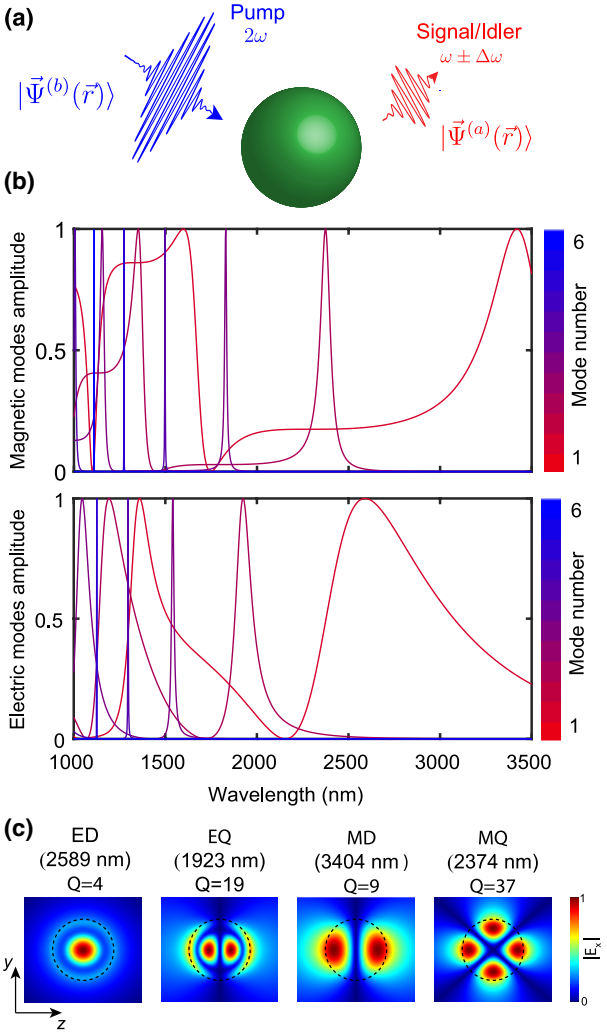

Fig. 2. OPO in a nanoscale dielectric sphere. (a) The resonator is composed of an AlGaAs spherical particle with a radius of 500 nm. A pump with a wavelength around the particle size can excite the multipolar modes of the particle. (b) Normalized scattering amplitude of the electric and magnetic modes. It is seen that for a broad portion of the spectrum, the particle supports multiple modes that spatially and spectrally overlap. (c) Normalized x component of the electric field for the first two electric and first two magnetic eigenmodes. If the pump is in the sub-wavelength regime (pump wavelength >1500 nm), the OPO signal can be a superposition of the lower-order modes. ED, electric dipole; EQ, electric quadrupole; MD, magnetic dipole; MQ, magnetic quadrupole. For excitations at shorter wavelengths, higher-order modes come into play as well. The resonant wavelength and the Q factor of the higher-order modes are reported in Supplement 1.

For a general case of dispersive or non-spherical three-dimensional resonators [Fig. 1(a)], we can use Lorentz reciprocity theory to find the quasi-normal modes of the resonator [51–54]. The details are reported in Supplement 1.

Figure 2(b) illustrates the normalized scattering coefficients for the first six electric and magnetic modes of a particle with a radius of 500 nm. If the particle is excited with a plane wave (or a Gaussian beam), several multipolar modes are excited. We first set the pump in the sub-wavelength regime (pump wavelength >1500 nm) where lower-order low-Q modes can be excited at signal and idler frequencies. Then we discuss the behavior of the OPO in the wavelength-scale (pump wavelength ≈1000 nm) regime where higher-order modes can also contribute.

If we operate in the sub-wavelength regime (i.e., the pump wavelength is larger than the particle size), only the first two electric and first two magnetic modes can oscillate in the down-conversion process. Higher-order modes can be neglected because of their large detuning ($\delta\omega_k \gg 1$). The electric field profiles of these four modes are illustrated in Fig. 2(c). The contribution of each mode in the OPO signal/idler supermode is dictated by the field overlap between the pump and the mode as well as the intermode nonlinear coupling as expressed in Eq. (2), the Q factor, and the detuning from the half-harmonic frequency. Figure 3 displays the oscillation threshold as well as the spectral separation of signal and idler as a function of the pump wavelength. The dip in the threshold spectrum around 1830 nm is due to the enhancement of the pump field as a result of the excitation of the third magnetic mode. Away from the center of the resonance, the input pump can still excite multiple lower-order modes of the resonator.

If we ignored the intermode coupling and assumed that only one of the eigenmodes can oscillate, the OPO threshold would be considerably higher. For instance, if the pump is at the center of the third magnetic resonance, the minimum threshold for the single-mode OPO is around 0.27 MW, which is 36 times higher than the threshold shown in Fig. 3(a) in which multi-mode interactions are taken into account (see Supplement 1 for the threshold of all modes and coupling coefficients). In traveling-wave multi-mode OPOs, it is understood that, in the best case scenario, the threshold is on the order of the single-mode threshold divided by the number of modes [31]. The reason is that the modes in traveling-wave resonators have the same nature. Thus, the maximum overlap is achieved if all the modes have the same mode profile [31,55]. However, in wavelength-scale OPOs, each of the multipolar modes has a different spatial distribution, and their overlap through the

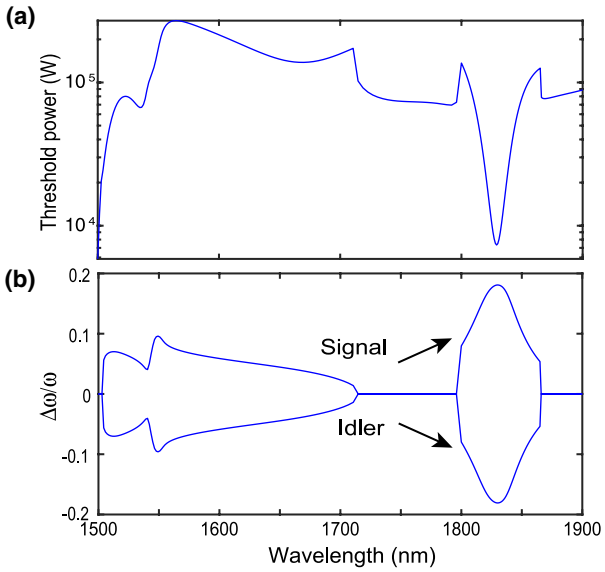

Fig. 3. Sub-wavelength OPO in a dielectric sphere. The structure is the same as that shown in Fig. 2. (a) Oscillation threshold as a function of the pump wavelength. The input is a plane wave that excites multiple modes of the resonator at the pump wavelength. (b) Signal and idler frequency separation ($\pm\Delta\omega$) from the half-harmonic frequency (ω) at the threshold as a function of the pump wavelength. The nonlinear interactions between the modes can reduce the threshold significantly. It can also cause a phase transition from degenerate ($\Delta\omega = 0$) to non-degenerate ($\Delta\omega \neq 0$), which results in a sudden change in the oscillation threshold.

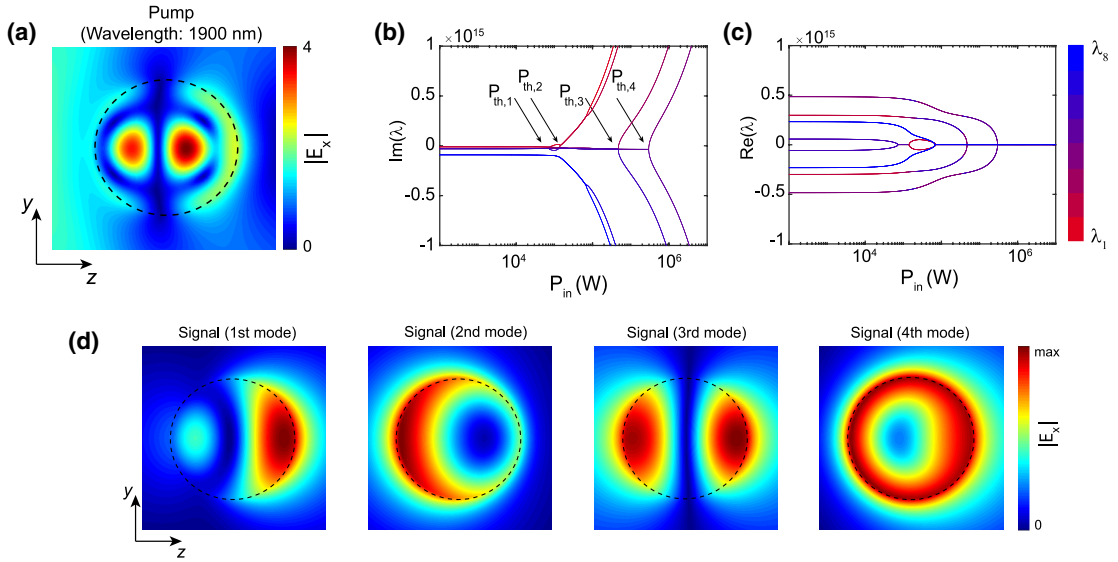

Fig. 4. Modes and eigenvalues in a sub-wavelength OPO in a dielectric sphere. (a) Electric field profile at pump wavelength (1900 nm) normalized to the amplitude of the plane-wave excitation. (b) Imaginary and (c) real parts of the eigenvalues as a function of the pump power. The eigenvalues are sorted based on their real part values. The imaginary and real parts correspond to the parametric gain and detuning from the half-harmonic ($\Delta\omega$), respectively. When the real part of the eigenvalues becomes positive, the parametric gain overcomes the loss. Hence, the down-converted signal can surpass the oscillation threshold. (d) Electric field profile of the signal supermodes. It is seen that even though the detuning for MQ mode at half-harmonic is significantly larger compared to ED and MD modes, the contribution of MQ mode on the first signal supermode is more evident. This is due to the stronger overlap between the pump mode and MQ mode. The strong nonlinear coupling between the signal eigenmodes helps to reduce the threshold 50 times compared to the case where we consider only one of the modes for the signal.

pump field can potentially lead to a strong coupling, even higher than the self-coupling (the diagonal terms of η_{lk}).

As seen in Fig. 3, when the OPO goes through a transition from non-degenerate to degenerate oscillation, there is a sudden drop in the threshold. This corresponds to a phase transition from disordered to ordered phases, which we have recently demonstrated in traveling-wave OPOs [56]. To understand the phase transition in wavelength-scale OPOs, we need to look at the eigenvalues and eigenvectors of these resonators. For instance, we focus on a degenerate case with a pump excitation at 1900 nm [Fig. 4(a)]. Figures 4(b) and4(c) display the real and imaginary parts of the eigenvalues as a function of the input power, respectively. Since four modes are involved at the signal and idler frequencies, there are eight eigenvalues and eight corresponding supermodes. The OPO threshold for each supermode is defined when the imaginary part of the eigenvalue passes zero [Fig. 4(b)].

At low input power levels, there is a weak coupling between the eigenmodes, as seen in Eq. (1). Hence, each supermode is dominated by a single eigenmode (see Supplement 1 for the eigenvectors). However, when the input power increases, the modes start to interact due to the nonlinear coupling through the pump. As a result, the supermodes near and above the threshold are a superposition of all eigenmodes. The electric field distributions of the four oscillating supermodes at the thresholds are shown in Fig. 4(d).

Moreover, due to the detuning of the center of resonance of the eigenmodes from the half-harmonic, the signal/idler supermodes for all eigenvalues are non-degenerate at low input power levels ($\mathrm{Re}(\lambda_m) \neq 0$) [Fig. 4(c)]. An increase in the input power enhances intermode coupling, which can change the signal and idler spectral separation. This can lead to a phase transition from non-degenerate to degenerate and vice versa. Especially at very high powers, the nonlinear coupling dominates the detuning [Eq. (1)], and as a result, all the modes are synchronized at the half-harmonic frequency [Fig. 4(c)].

The phase transition in the largest eigenvalue is illustrated in Fig. 5. This phase transition is accompanied by an abrupt change in the slope of the parametric gain [56,57], which can be utilized for enhanced sensing and computing [58,59]. A phase transition can happen due to either the competition between eigenvalues to achieve the highest gain or the coalescence of two eigenvalues. If a critical point is a coalescence of two eigenvalues, the eigenvectors coalesce as well at the critical point (see Supplement 1), which

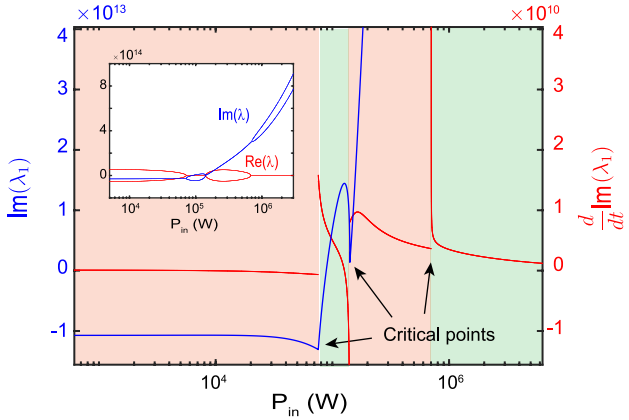

Fig. 5. Phase transition in wavelength-scale OPOs. The imaginary part of the largest eigenvalue (blue) and its derivative for the structure shown in Fig. 4. The inset shows both real and imaginary parts of the two eigenvalues with the smallest real parts, which correspond to λ_1 and λ_2 for most of the input powers. When there is a transition from degenerate (green) to non-degenerate (red), there is an abrupt change in the parametric gain at the critical points. The discontinuities in the derivative of the parametric gain corresponds to phase transitions in OPO. When two eigenvalues coalesce at a critical point, the derivative of the parametric gain diverges.

is a signature of exceptional points in non-Hermitian systems [60–63]. We have recently shown first-order phase transition in coupled OPOs [56]. However, the phase transition proposed here is observed in a single wavelength-scale OPO due to the strong nonlinear coupling between the multiple modes of the resonator.

To improve the performance of OPOs, it is desired to reduce the oscillation threshold further. The OPO threshold is inversely proportional to the Q factor of the pump mode if only one mode exists at the pump frequency (see Supplement 1). Hence, it is expected to reduce the threshold further by exciting the higher-order modes, as the higher-order multipolar modes have even higher Q factors. Figure 6(a) shows the OPO threshold for the first oscillating supermode as a function of the pump wavelength around the sixth magnetic mode at 1110 nm with a Q factor of 10^4 and the fifth electric mode at 1125 nm with a Q factor of 2500. The seperation of the signal/idler frequencies from the half-harmonic is shown in Fig. 6(b). For the signal and idler, we have considered all the modes with a resonant wavelength longer than the pump wavelength (the first four electric and first five magnetic modes). The electric field distributions for the pump as well as the first signal/idler supermodes for magnetic and electric mode excitations are shown in Figs. 6(c) and 6(d), respectively. The threshold at the center of the resonance of the sixth magnetic mode and the fifth electric mode can reach down to 2 W and 460 W, respectively. Due to the large signal and idler separation, the parametric gain is low. However, at input power of 43 W around the sixth magnetic mode and input power of 1900 W around the fifth electric mode, the OPO experiences a phase transition into the degenerate regime, and the parametric gain is dramatically enhanced (see Supplement 1). Note that for the fifth electric mode, even though the Q is large and high-Q modes can also be excited at the signal wavelength, the threshold is not significantly different from the sub-wavelength regime shown in Fig. 3. This is because of a weaker field overlap between the pump and the signal modes in the absence of phase matching in larger resonators. It is seen in Fig. 6(b) that because of the competition between different eigenvalues, a phase transition can happen in the non-degenerate regime with a sudden change in the signal/idler spectral separation resulting in a discontinuous change in the derivative of the OPO threshold, as shown in Fig. 6(a).

The approach that we have used to estimate the threshold can also be applied to estimate the SHG in multi-mode wavelength-scale resonators (see Supplement 1 for more details). Specifically, in the simple case that the pump and signal are single mode, we arrive at a simple relationship between the OPO threshold and the SHG efficiency ($\epsilon_{\mathrm{SHG}} = P_{\mathrm{out}}/P_{\mathrm{in}}^2$, where P_{in} and P_{out} are the input power at the fundamental harmonic and the output power at the second harmonic, respectively), which can be expressed as

$$P_{\mathrm{th}} = \frac{4\alpha^{(a)2}}{\alpha^{(b)2}\epsilon_{\mathrm{SHG}}}\left(\frac{\frac{\alpha^{(b)2}}{4}+\delta\omega^{(b)2}}{\frac{\alpha^{(a)2}}{4}+\delta\omega^{(a)2}}\right) \approx \frac{4}{\epsilon_{\mathrm{SHG}}}. \tag{5}$$

As there is no threshold for the SHG process and conventional detectors are more sensitive at shorter wavelengths [64], it is usually easier to simulate or measure the SHG signal. This allows us to estimate the OPO threshold in some structures that have already been proposed for SHG. Figure 7 displays a few examples and the estimated threshold in these structures. The low threshold in the inversely designed structure [65] (compared to the photonic crystal structure with a higher Q factor [66]) shows the importance of the field overlap to achieve a strong nonlinear response. Note that the thresholds reported in Fig. 7 are for a continuous-wave sources.

Since the round-trip time in wavelength-scale OPOs is only a few femtoseconds and the Q factor compared to micro-resonators is relatively low, the input pump can be compressed in time into a short pulse. This can lead to average-power thresholds of a few tens of milliwatts (with a pulse repetition rate of 100 MHz) even for subwavelength OPOs, which is on the order of the threshold for free-space pulsed OPOs [4,8]. Hence, the oscillation can happen before the onset of the material damage threshold. The field overlap can be further enhanced by Mie resonance engineering [67], inverse design [68], using hybrid plasmonic structures [26], or controlling evanescent waves [69]. This can potentially help to

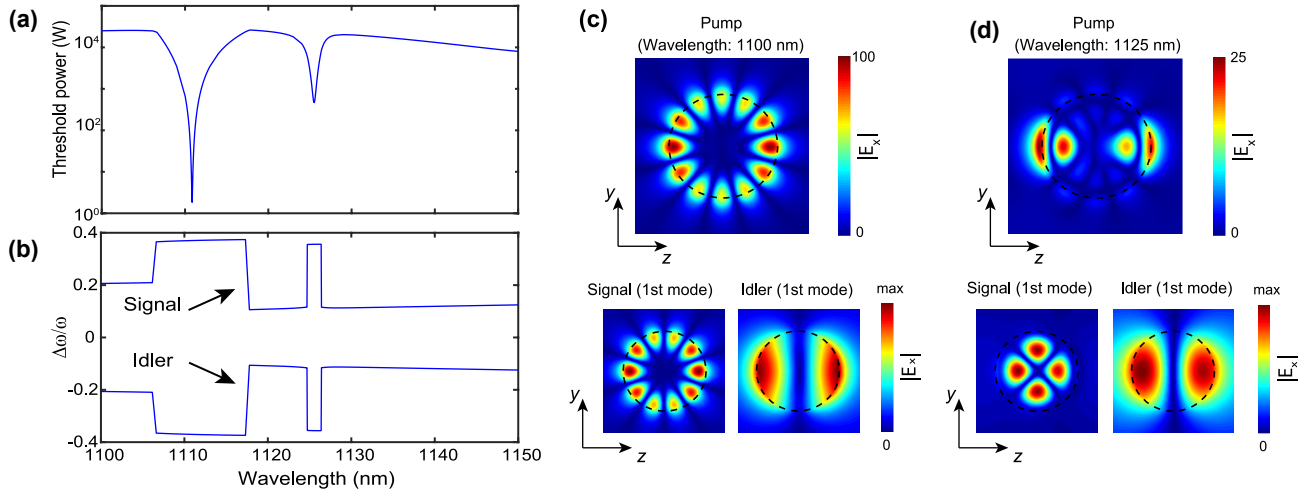

Fig. 6. Wavelength-scale OPO. (a) OPO threshold as a function of the pump wavelength. The dips in the threshold around 1110 nm and 1125 nm correspond to the sixth magnetic mode and the fifth electric mode, respectively. The Q factors for these modes are 10^4 and 2500, respectively. The first four electric modes and the first five magnetic modes are considered as the eigenmodes for signal and idler modes. (b) Normalized detuning of the signal and idler from the half-harmonic at the threshold. Spectral phase transition can be observed leading to a sudden change in $\Delta\omega$ and a discontinuity in the derivative of the threshold. (c) Electric field distribution for the pump and the first signal/idler supermodes when the pump is at 1110 nm. (d) Electric field distribution for the pump and the first signal/idler supermodes when the pump is at 1125 nm.

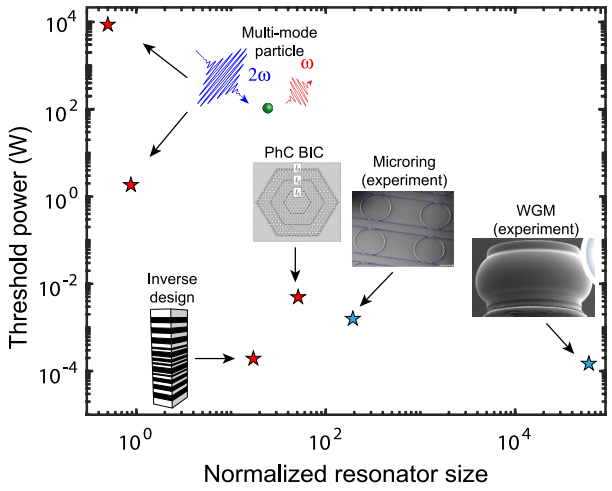

Fig. 7. Estimation of the OPO threshold in various platforms. Estimation of the threshold in a single-mode photonic crystal [66] and inversely designed cavities [65] is based on the reported value for the SHG efficiency. The sizes of resonators are normalized to the pump wavelength. As a reference, we have included OPOs demonstrated experimentally based on microring [21] and whispering-gallery mode (WGM) [22] resonators.

achieve a sub-milliwatt oscillation threshold in subwavelength and wavelength-scale resonators.

4. CONCLUSION

In conclusion, we proposed a general theory to estimate the oscillation threshold in wavelength-scale OPOs and the nonlinear mixing behavior of modes above the threshold. We showed that the nonlinear interactions in multi-mode wavelength-scale resonators can be different from their large-scale counterparts, and the threshold can be reduced considerably as a result of multi-mode interactions in these resonators. We demonstrated a phase transition in these resonators due to the nonlinear interactions between multiple modes. We have shown that although the phase matching is not required in this regime, the field overlap between modes can play a crucial role in reducing the threshold. Our formalism is general and can predict the behavior of OPOs above the threshold if the pump depletion is also taken into account. It can also be applied to $\chi^{(3)}$ cavities. Our approach can enable the design of a new class of nonlinear integrated photonic systems.

Funding. National Science Foundation (1846273, 1918549); Army Research Office (W911NF- 18-1-0285).

Acknowledgment. We thank Philippe Lalanne for valuable comments. The authors thank NTT Research for financial and technical support.

Disclosures. The authors declare no conflicts of interest.

Supplemental document. See Supplement 1 for supporting content.

REFERENCES

1. R. C. Eckardt, C. Nabors, W. J. Kozlovsky, and R. L. Byer, "Optical parametric oscillator frequency tuning and control," J. Opt. Soc. Am. B **8**, 646–667 (1991).
2. A. Schliesser, N. Picqué, and T. W. Hänsch, "Mid-infrared frequency combs," Nat. Photonics **6**, 440–449 (2012).
3. I. Breunig, "Three-wave mixing in whispering gallery resonators," Laser Photon. Rev. **10**, 569–587 (2016).
4. A. Marandi, N. C. Leindecker, V. Pervak, R. L. Byer, and K. L. Vodopyanov, "Coherence properties of a broadband femtosecond mid-IR optical parametric oscillator operating at degeneracy," Opt. Express **20**, 7255–7262 (2012).
5. T. Kippenberg, S. Spillane, and K. Vahala, "Kerr-nonlinearity optical parametric oscillation in an ultrahigh-Q toroid microcavity," Phys. Rev. Lett. **93**, 083904 (2004).
6. Y. Okawachi, M. Yu, K. Luke, D. O. Carvalho, S. Ramelow, A. Farsi, M. Lipson, and A. L. Gaeta, "Dual-pumped degenerate Kerr oscillator in a silicon nitride microresonator," Opt. Lett. **40**, 5267–5270 (2015).
7. T. Inagaki, K. Inaba, R. Hamerly, K. Inoue, Y. Yamamoto, and H. Takesue, "Large-scale Ising spin network based on degenerate optical parametric oscillators," Nat. Photonics **10**, 415–419 (2016).
8. A. Muraviev, V. Smolski, Z. Loparo, and K. Vodopyanov, "Massively parallel sensing of trace molecules and their isotopologues with broadband subharmonic mid-infrared frequency combs," Nat. Photonics **12**, 209–214 (2018).
9. J. Roslund, R. M. De Araujo, S. Jiang, C. Fabre, and N. Treps, "Wavelength-multiplexed quantum networks with ultrafast frequency combs," Nat. Photonics **8**, 109–112 (2014).
10. G. Milburn and D. Walls, "Production of squeezed states in a degenerate parametric amplifier," Opt. Commun. **39**, 401–404 (1981).
11. L.-A. Wu, H. J. Kimble, J. L. Hall, and H. Wu, "Generation of squeezed states by parametric down conversion," Phys. Rev. Lett. **57**, 2520 (1986).
12. M. Chen, N. C. Menicucci, and O. Pfister, "Experimental realization of multipartite entanglement of 60 modes of a quantum optical frequency comb," Phys. Rev. Lett. **112**, 120505 (2014).
13. O. Morin, K. Huang, J. Liu, H. Le Jeannic, C. Fabre, and J. Laurat, "Remote creation of hybrid entanglement between particle-like and wave-like optical qubits," Nat. Photonics **8**, 570–574 (2014).
14. R. Nehra, A. Win, M. Eaton, R. Shahrokhshahi, N. Sridhar, T. Gerrits, A. Lita, S. W. Nam, and O. Pfister, "State-independent quantum state tomography by photon-number-resolving measurements," Optica **6**, 1356–1360 (2019).
15. A. Marandi, Z. Wang, K. Takata, R. L. Byer, and Y. Yamamoto, "Network of time-multiplexed optical parametric oscillators as a coherent Ising machine," Nat. Photonics **8**, 937–942 (2014).
16. P. L. McMahon, A. Marandi, Y. Haribara, R. Hamerly, C. Langrock, S. Tamate, T. Inagaki, H. Takesue, S. Utsunomiya, K. Aihara, R. L. Byer, M. M. Fejer, H. Mabuchi, and Y. Yamamoto, "A fully programmable 100-spin coherent Ising machine with all-to-all connections," Science **354**, 614–617 (2016).
17. Y. Okawachi, M. Yu, J. K. Jang, X. Ji, Y. Zhao, B. Y. Kim, M. Lipson, and A. L. Gaeta, "Demonstration of chip-based coupled degenerate optical parametric oscillators for realizing a nanophotonic spin-glass," Nat. Commun. **11**, 4119 (2020).
18. C. Wang, C. Langrock, A. Marandi, M. Jankowski, M. Zhang, B. Desiatov, M. M. Fejer, and M. Lončar, "Ultrahigh-efficiency wavelength conversion in nanophotonic periodically poled lithium niobate waveguides," Optica **5**, 1438–1441 (2018).
19. D. M. Lukin, C. Dory, M. A. Guidry, K. Y. Yang, S. D. Mishra, R. Trivedi, M. Radulaski, S. Sun, D. Vercruysse, G. H. Ahn, and J. Vučković, "4H-silicon-carbide-on-insulator for integrated quantum and nonlinear photonics," Nat. Photonics **14**, 330–334 (2020).
20. C. Conti, A. Di Falco, and G. Assanto, "Optical parametric oscillations in isotropic photonic crystals," Opt. Express **12**, 823–828 (2004).
21. A. W. Bruch, X. Liu, J. B. Surya, C.-L. Zou, and H. X. Tang, "On-chip $\chi(2)$ microring optical parametric oscillator," Optica **6**, 1361–1366 (2019).
22. C. S. Werner, T. Beckmann, K. Buse, and I. Breunig, "Blue-pumped whispering gallery optical parametric oscillator," Opt. Lett. **37**, 4224–4226 (2012).
23. D. Smirnova and Y. S. Kivshar, "Multipolar nonlinear nanophotonics," Optica **3**, 1241–1255 (2016).
24. S. Jahani and Z. Jacob, "Transparent subdiffraction optics: nanoscale light confinement without metal," Optica **1**, 96–100 (2014).
25. F. Monticone and A. Alu, "Embedded photonic eigenvalues in 3D nanostructures," Phys. Rev. Lett. **112**, 213903 (2014).
26. M. P. Nielsen, X. Shi, P. Dichtl, S. A. Maier, and R. F. Oulton, "Giant nonlinear response at a plasmonic nanofocus drives efficient four-wave mixing," Science **358**, 1179–1181 (2017).
27. O. Reshef, I. De Leon, M. Z. Alam, and R. W. Boyd, "Nonlinear optical effects in epsilon-near-zero media," Nat. Rev. Mater. **4**, 535–551 (2019).

28. Y. Yang, J. Lu, A. Manjavacas, T. S. Luk, H. Liu, K. Kelley, J.-P. Maria, E. L. Runnerstrom, M. B. Sinclair, S. Ghimire, and I. Brener, "High-harmonic generation from an epsilon-near-zero material," Nat. Phys. **15**, 1022–1026 (2019).
29. R. Hamerly, A. Marandi, M. Jankowski, M. M. Fejer, Y. Yamamoto, and H. Mabuchi, "Reduced models and design principles for half-harmonic generation in synchronously pumped optical parametric oscillators," Phys. Rev. A **94**, 063809 (2016).
30. T. Herr, V. Brasch, J. D. Jost, C. Y. Wang, N. M. Kondratiev, M. L. Gorodetsky, and T. J. Kippenberg, "Temporal solitons in optical microresonators," Nat. Photonics **8**, 145–152 (2014).
31. G. J. De Valcarcel, G. Patera, N. Treps, and C. Fabre, "Multimode squeezing of frequency combs," Phys. Rev. A **74**, 061801 (2006).
32. A. N. Poddubny and D. A. Smirnova, "Nonlinear generation of quantum-entangled photons from high-Q states in dielectric nanoparticles," arXiv:1808.04811 (2018).
33. A. Nikolaeva, K. Frizyuk, N. Olekhno, A. Solntsev, and M. Petrov, "Directional emission of down-converted photons from a dielectric nano-resonator," arXiv:2011.07842 (2020).
34. A. Ciattoni, A. Marini, C. Rizza, and C. Conti, "Phase-matching-free parametric oscillators based on two-dimensional semiconductors," Light Sci. Appl. **7**, 5 (2018).
35. H. A. Haus, *Waves and Fields in Optoelectronics* (Prentice-Hall, 1984).
36. C. Fabre, E. Giacobino, A. Heidmann, L. Lugiato, S. Reynaud, M. Vadacchino, and W. Kaige, "Squeezing in detuned degenerate optical parametric oscillators," Quantum Opt. J. Eur. Opt. Soc. Part B **2**, 159 (1990).
37. A. Rodriguez, M. Soljačić, J. D. Joannopoulos, and S. G. Johnson, "$\chi(2)$ and $\chi(3)$ harmonic generation at a critical power in inhomogeneous doubly resonant cavities," Opt. Express **15**, 7303–7318 (2007).
38. S. Jahani and Z. Jacob, "All-dielectric metamaterials," Nat. Nanotechnology **11**, 23 (2016).
39. A. I. Kuznetsov, A. E. Miroshnichenko, M. L. Brongersma, Y. S. Kivshar, and B. Luk'yanchuk, "Optically resonant dielectric nanostructures," Science **354**, aag2472 (2016).
40. D. G. Baranov, D. A. Zuev, S. I. Lepeshov, O. V. Kotov, A. E. Krasnok, A. B. Evlyukhin, and B. N. Chichkov, "All-dielectric nanophotonics: the quest for better materials and fabrication techniques," Optica **4**, 814–825 (2017).
41. A. Krasnok, M. Tymchenko, and A. Alù, "Nonlinear metasurfaces: a paradigm shift in nonlinear optics," Mater. Today **21**(1), 8–21 (2018).
42. T. Pertsch and Y. Kivshar, "Nonlinear optics with resonant metasurfaces," MRS Bull. **45**(3), 210–220 (2020).
43. S. Liu, M. B. Sinclair, S. Saravi, G. A. Keeler, Y. Yang, J. Reno, G. M. Peake, F. Setzpfandt, I. Staude, T. Pertsch, and I. Brener, "Resonantly enhanced second-harmonic generation using III–V semiconductor all-dielectric metasurfaces," Nano Lett. **16**, 5426–5432 (2016).
44. L. Carletti, K. Koshelev, C. De Angelis, and Y. Kivshar, "Giant nonlinear response at the nanoscale driven by bound states in the continuum," Phys. Rev. Lett. **121**, 033903 (2018).
45. G. Marino, A. S. Solntsev, L. Xu, V. F. Gili, L. Carletti, A. N. Poddubny, M. Rahmani, D. A. Smirnova, H. Chen, A. Lematre, G. Zhang, A. V. Zayats, C. De Angelis, G. Leo, A. A. Sukhorukov, and D. N. Neshev, "Spontaneous photon-pair generation from a dielectric nanoantenna," Optica **6**, 1416–1422 (2019).
46. M. Timofeeva, L. Lang, F. Timpu, C. Renaut, A. Bouravleuv, I. Shtrom, G. Cirlin, and R. Grange, "Anapoles in free-standing III–V nanodisks enhancing second-harmonic generation," Nano Lett. **18**, 3695–3702 (2018).
47. K. Koshelev, S. Kruk, E. Melik-Gaykazyan, J.-H. Choi, A. Bogdanov, H.-G. Park, and Y. Kivshar, "Subwavelength dielectric resonators for nonlinear nanophotonics," Science **367**, 288–292 (2020).
48. C. Gigli, T. Wu, G. Marino, A. Borne, G. Leo, and P. Lalanne, "Quasinormal-mode non-Hermitian modeling and design in nonlinear nano-optics," ACS Photon. **7**, 1197–1205 (2020).
49. V. Gili, L. Carletti, A. Locatelli, D. Rocco, M. Finazzi, L. Ghirardini, I. Favero, C. Gomez, A. Lematre, M. Celebrano, C. De Angelis, and G. Leo, "Monolithic AlGaAs second-harmonic nanoantennas," Opt. Express **24**, 15965–15971 (2016).
50. S. Buckley, M. Radulaski, J. L. Zhang, J. Petykiewicz, K. Biermann, and J. Vučković, "Multimode nanobeam cavities for nonlinear optics: high quality resonances separated by an octave," Opt. Express **22**, 26498–26509 (2014).
51. C. Sauvan, J.-P. Hugonin, I. Maksymov, and P. Lalanne, "Theory of the spontaneous optical emission of nanosize photonic and plasmon resonators," Phys. Rev. Lett. **110**, 237401 (2013).
52. A. Raman and S. Fan, "Photonic band structure of dispersive metamaterials formulated as a Hermitian eigenvalue problem," Phys. Rev. Lett. **104**, 087401 (2010).
53. P. Lalanne, W. Yan, K. Vynck, C. Sauvan, and J.-P. Hugonin, "Light interaction with photonic and plasmonic resonances," Laser Photon. Rev. **12**, 1700113 (2018).
54. W. Yan, R. Faggiani, and P. Lalanne, "Rigorous modal analysis of plasmonic nanoresonators," Phys. Rev. B **97**, 205422 (2018).
55. G. Alves, R. Barros, D. Tasca, C. Souza, and A. Khoury, "Conditions for optical parametric oscillation with a structured light pump," Phys. Rev. A **98**, 063825 (2018).
56. A. Roy, S. Jahani, C. Langrock, M. Fejer, and A. Marandi, "Spectral phase transitions in optical parametric oscillators," arXiv:2009.00930 (2020).
57. K. B. Arnardottir, A. J. Moilanen, A. Strashko, P. Törmä, and J. Keeling, "Multimode organic polariton lasing," Phys. Rev. Lett. **125**, 233603 (2020).
58. F. Arute, K. Arya, R. Babbush, D. Bacon, J. C. Bardin, R. Barends, R. Biswas, S. Boixo, F. G. Brandao, D. A. Buell, B. Burkett, Y. Chen, Z. Chen, B. Chiaro, R. Collins, W. Courtney, A. Dunsworth, E. Farhi, B. Foxen, A. Fowler, C. Gidney, M. Giustina, R. Graff, K. Guerin, S. Habegger, M. P. Harrigan, M. J. Hartmann, A. Ho, M. Hoffmann, T. Huang, T. S. Humble, S. V. Isakov, E. Jeffrey, Z. Jiang, D. Kafri, K. Kechedzhi, J. Kelly, P. V. Klimov, S. Knysh, A. Korotkov, F. Kostritsa, D. Landhuis, M. Lindmark, E. Lucero, D. Lyakh, S. Mandrà, J. R. McClean, M. McEwen, A. Megrant, X. Mi, K. Michielsen, M. Mohseni, J. Mutus, O. Naaman, M. Neeley, C. Neill, M. Y. Niu, E. Ostby, A. Petukhov, J. C. Platt, C. Quintana, E. G. Rieffel, P. Roushan, N. C. Rubin, D. Sank, K. J. Satzinger, V. Smelyanskiy, K. J. Sung, M. D. Trevithick, A. Vainsencher, B. Villalonga, T. White, Z. J. Yao, P. Yeh, A. Zalcman, H. Neven, and J. M. Martinis, "Quantum supremacy using a programmable superconducting processor," Nature **574**, 505–510 (2019).
59. L. P. Yang and Z. Jacob, "Single-photon pulse induced giant response in N > 100 qubit system," npj Quantum Inform. **6**, 1–6 (2020).
60. A. Roy, S. Jahani, Q. Guo, A. Dutt, S. Fan, M.-A. Miri, and A. Marandi, "Non-dissipative non-Hermitian dynamics and exceptional points in coupled optical parametric oscillators," arXiv:2009.07522 (2020).
61. M.-A. Miri and A. Alu, "Exceptional points in optics and photonics," Science **363**, eaar7709 (2019).
62. M. Parto, Y. G. Liu, B. Bahari, M. Khajavikhan, and D. N. Christodoulides, "Non-Hermitian and topological photonics: optics at an exceptional point," Nanophotonics **10**, 403–423 (2020).
63. Y. Lumer, Y. Plotnik, M. C. Rechtsman, and M. Segev, "Nonlinearly induced PT transition in photonic systems," Phys. Rev. Lett. **111**, 263901 (2013).
64. R. H. Hadfield, "Single-photon detectors for optical quantum information applications," Nat. Photonics **3**, 696–705 (2009).
65. Z. Lin, X. Liang, M. Lončar, S. G. Johnson, and A. W. Rodriguez, "Cavity-enhanced second-harmonic generation via nonlinear-overlap optimization," Optica **3**, 233–238 (2016).
66. M. Minkov, D. Gerace, and S. Fan, "Doubly resonant $\chi(2)$ nonlinear photonic crystal cavity based on a bound state in the continuum," Optica **6**, 1039–1045 (2019).
67. J. H. Bahng, S. Jahani, D. Montjoy, T. Yao, N. Kotov, and A. Marandi, "Mie resonance engineering in meta-shell supraparticles for nanoscale nonlinear optics," ACS Nano **14**, 17203–17212 (2020).
68. S. Molesky, Z. Lin, A. Y. Piggott, W. Jin, J. Vucković, and A. W. Rodriguez, "Inverse design in nanophotonics," Nat. Photonics **12**, 659–670 (2018).
69. S. Jahani, S. Kim, J. Atkinson, J. C. Wirth, F. Kalhor, A. Al Noman, W. D. Newman, P. Shekhar, K. Han, V. Van, R. G. DeCorby, L. Chrostowski, M. Qi, and Z. Jacob, "Controlling evanescent waves using silicon photonic all-dielectric metamaterials for dense integration," Nat. Commun. **9**, 18 (2018).